NOAA Technical Memorandum ERL WPL-190

OCEAN SURFACE CURRENT MEASUREMENTS WITH A SINGLE-STATION, DOPPLER/SPACED-ANTENNA RADAR

B. L. Weber
D. B. Wuertz
P. T. May
R. G. Strauch
D. A. Merritt
K. P. Moran

Wave Propagation Laboratory
Boulder, Colorado
November 1990

noaa NATIONAL OCEANIC AND ATMOSPHERIC ADMINISTRATION / Environmental Research Laboratories

NOAA Technical Memorandum ERL WPL-190

OCEAN SURFACE CURRENT MEASUREMENTS WITH A SINGLE-STATION, DOPPLER/SPACED-ANTENNA RADAR

B. L. Weber
D. B. Wuertz
P. T. May
R. G. Strauch
D. A. Merritt
K. P. Moran

Wave Propagation Laboratory
Boulder, Colorado
November 1990

UNITED STATES DEPARTMENT OF COMMERCE

Robert A. Mosbacher
Secretary

NATIONAL OCEANIC AND ATMOSPHERIC ADMINISTRATION

John A. Knauss
Under Secretary for Oceans and Atmosphere/Administrator

Environmental Research Laboratories

Joseph O. Fletcher
Director

NOTICE

Mention of a commercial company or product does not constitute an endorsement by NOAA/Environmental Research Laboratories. Use of information from this publication concerning proprietary products or tests of such products for publicity or advertising purposes is not authorized.

For sale by the National Technical Information Service, 5285 Port Royal Road
Springfield, VA 22161

CONTENTS

Ocean Surface Current Measurements with a Single-Station, Doppler/Spaced-Antenna Radar

B.L. Weber, D.B. Wuertz, P.T. May, R.G. Strauch, D.A. Merritt, and K.P. Moran

ABSTRACT. We conducted a preliminary experiment to determine the feasibility of using one radar to measure the two-dimensional ocean surface current. The Doppler method was used to measure the radial component and the Spaced Antenna (SA) method was used to measure the transverse component of the current. This dual method produced current measurements that showed consistency over range and time, demonstrating potential for the technique. However, the experiment also raised some questions. On occasions, the SA method seemed to be very sensitive to noise, producing apparently erroneous results. Therefore, we have planned a more definitive experiment with improved radar antennas, with improved data acquisition, and with independent current observations for comparisons.

1. INTRODUCTION

Ocean surface currents have been observed remotely with Doppler radars for decades. During the 1970s and 1980s, modest power, shore-based HF radars were developed to measure ocean surface currents out to ranges of 50 km using ground-wave propagation (Frisch and Weber, 1982; Frisch and Weber, 1980; Barrick et al., 1977). These could monitor coastal circulation continuously in time over approximately 1000 km^2 with two radar units separated by about 25 km. Two separated radar sites are necessary in order to measure both components of the surface current because Doppler radars only measure the radial component of the current.

Now the Wave Propagation Laboratory (WPL) is engaged in determining whether one radar station can provide both components of the surface current (May, 1989). If that is possible, some of the advantages are obvious. The radar hardware costs, the maintenance requirements, inter-site data communications, and the demands upon personnel are reduced. But, more important, it would create some new applications, e.g., when only one site is available, as on offshore oil platforms and along rugged or otherwise restricted coastlines.

The single-station radar would use the Doppler method to measure the radial component and the SA method (Briggs, 1984; Vincent et al., 1987; Larsen and Röttger, 1989) to measure the transverse component of the ocean surface current. Both methods have been used successfully for years to measure winds in the atmosphere (Briggs, 1980; May et al.,

1988; May, 1990). The Doppler method (Strauch et al., 1987; Wuertz et al., 1988; Weber and Wuertz, 1990) and the SA method (May, 1988; Hocking et al., 1989) can produce reliable, accurate wind measurements.

In November 1988, WPL conducted an experiment off the coast of Santa Barbara, California, using radar equipment borrowed from one of its VHF (49.8 MHz, $\lambda = 6$ m) wind profilers from the Colorado network. Instead of looking upwards into the atmosphere though, the radar looked horizontally out over the ocean.

The antennas were different from those used in wind profiling. A simple five-element Yagi antenna was used for transmitting and two linear arrays of whips for receiving. The transmitting antenna was located midway between the two receiving antennas and all antennas were situated on a cliff about 120 feet above mean sea level. All had their boresights pointing in the same direction, 151.5° counterclockwise relative to true north. Several different sizes of receiving arrays separated by different distances were used. In this paper, we report only data collected with two receiving arrays, each of four elements spaced $\lambda/2$ apart and separated by 2λ. With such small arrays, the receiver beamwidths were very broad (about 30°), too broad for some of the interesting flows that can exist in the Santa Barbara Channel. This is one deficiency that will be corrected in future experiments.

Data acquisition was identical, in principle, to that used in wind profiling except the sample interval was larger (about 0.5 sec) and longer time series (512 points) were used to compute Doppler spectra. This reduced the largest measurable velocity from that used in wind profiling applications, while increasing the velocity resolution. Both timing changes were necessary because the largest velocities in the ocean are smaller than those in the atmosphere. The Doppler spectral width was $\pm$ 1 Hz, which was suitable for the .75 Hz Bragg frequency of the 3 m ocean waves doing the backscattering with the low currents observed in this experiment. However, larger currents would produce larger Doppler shifts, requiring wider spectra. That can be accomplished by reducing the sample time interval. Just over 4 minutes of data were collected in this way every 15 min from 0530 to 1445 UTC on 16 November 1988. In the next experiment, we shall record data continuously over the hour to provide many more Doppler spectra for averaging.

Because of computer memory limitations, data were collected only at six ranges along the boresights of the antennas, starting at 1.45 km from shore and at 0.9 km intervals out to 5.95 km. Greater ranges could have been easily achieved since the peak signal-to-noise ratio at the farthest range exceeded 30 dB. In the next experiment, we plan to have many more range gates along with beam steering to give measurements over the total offshore coverage area of the radar.

The main purpose of the present paper is to demonstrate with measurements and analysis how the dual Doppler/SA method works. In the process, we reveal some of the potential weaknesses of the SA technique when applied to complicated circulations in coastal waters. This in no way diminishes the need for further experimentation and

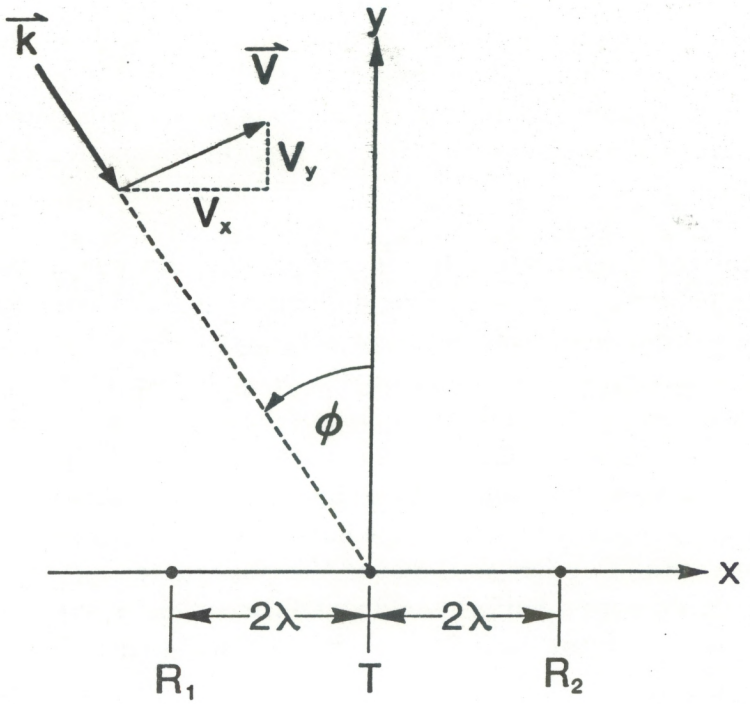

Fig. 1. Radar geometry showing the positions of the first (R_1) and second (R_2) receiving antennas relative to the transmitting antenna (T). All three antenna boresights are parallel and directed along the y-axis. Radar backscatter comes from all illuminated parts of the sea surface at each angle ϕ within the antenna beam. That angle also gives the direction of propagation for a backscattering ocean surface wave whose wavevector is $\boldsymbol{k}$. The ocean surface current velocity $\boldsymbol{v}$ is shown with its transverse v_x and parallel v_y components.

analysis, however, because the benefits are great if the technique can be made to work with acceptable accuracy and resolution to measure ocean surface currents.

2. THEORY

The Doppler spectrum and the cross spectrum for one range cell are modelled as follows (see Appendix):

$$S(\omega) \sim \int d\phi \; exp\Big(-\frac{\phi^2}{2\phi_o^2}\Big) \; exp\big(i\boldsymbol{k}\cdot\boldsymbol{r}_{12}/2\big)$$
$$\Big\{s_+ \; exp\Big(-\frac{(\omega-\omega_B-\boldsymbol{k}\cdot\boldsymbol{v})^2}{2\omega_o^2}\Big) + s_- \; exp\Big(-\frac{(\omega+\omega_B-\boldsymbol{k}\cdot\boldsymbol{v})^2}{2\omega_o^2}\Big)\Big\} \tag{1}$$

where S is the spectral density at the Doppler frequency ω, where ω_B is the Bragg frequency, $\boldsymbol{k}$ is the wavevector of the ocean surface wave doing the scattering, and $\boldsymbol{v}$ is the

ocean surface current velocity vector. This spectrum is a function of the integrated contributions from all parts of the ocean within the antenna beam, where ϕ is the angle-of-arrival, positive counterclockwise from antenna boresight (Fig. 1), which is perpendicular to the baseline of the receiver antennas. As it stands, this expression gives the cross spectrum. The Doppler spectrum is obtained by setting to zero $\boldsymbol{r}_{12}$, the separation of the two receiver antennas.

The first exponential function gives the Gaussian antenna beam pattern, where ϕ_o equals the two-way full beamwidth at half power divided by $\sqrt{8ln2}$. The second exponential function gives the phase difference between the two receiver antennas, where $\boldsymbol{k}$ is the ocean surface wave wavevector and $\boldsymbol{r}_{12}$ is a vector giving the relative positions of the two receiving antennas. The next two terms give returned signals backscattered from advancing and receding ocean surface waves, respectively, with wave energies of s_+ and s_-, which are assumed to be uniform across the range cell. The exponential factors in each of those terms give the Gaussian Doppler line shapes for each backscattering direction within the range cell, where ω_B gives the Doppler shift due to the phase velocity of a Bragg wave, and $\boldsymbol{k}\cdot\boldsymbol{v}$ gives the Doppler shift due to a uniform ocean surface current $\boldsymbol{v}$ in the scattering patch. Doppler broadening due to current variations within the scattering patch is described by ω_o.

By assuming that the transmitter and receiver antenna beams are not too wide, we can make the small angle approximation so that

$$\begin{aligned} \boldsymbol{k}\cdot\boldsymbol{v} &= k\, v_x\, sin\phi \;-\; k\, v_y\, cos\phi \;\simeq k\, v_x\, \phi \;-\; k\, v_y \\ \boldsymbol{k}\cdot\boldsymbol{r}_{12}/2 &= -\, k\, d\, sin\phi \;\simeq\; -\, k\, d\, \phi \end{aligned} \tag{2}$$

where v_x is the transverse velocity (positive to the right) and v_y is the radial velocity (positive away from the radar). The separation between the two receiver antennas is $2d$. If the antenna beam is too wide, then the full analysis (see Appendix) must be used.

Since we are interested in velocity measurements, it is useful to convert the various frequencies with the following identities.

$$\begin{aligned} \omega &= k\, v \\ \omega_B &= k\, v_B \\ \omega_o &= k\, v_o \end{aligned} \tag{3}$$

where v is the Doppler velocity, v_B is the Bragg velocity, and v_o gives the Doppler velocity broadening.

Then the integral (1) can be evaluated to give

$$S(v) \sim \frac{\sqrt{2\pi} v_o \phi_o}{\sqrt{v_o^2 + v_x^2 \phi_o^2}} \; exp\Big(-\frac{(k d v_o \phi_o)^2}{2(v_o^2 + v_x^2 \phi_o^2)}\Big)$$

$$\Big\{ s_+ \; exp\Big(-\frac{(v - v_B + v_y)^2}{2(v_o^2 + v_x^2 \phi_o^2)}\Big) \; exp\Big(-i \frac{k d v_x (v - v_B + v_y) \phi_o^2}{(v_o^2 + v_x^2 \phi_o^2)}\Big) \tag{4}$$

$$+ s_- \; exp\Big(-\frac{(v + v_B + v_y)^2}{2(v_o^2 + v_x^2 \phi_o^2)}\Big) \; exp\Big(-i \frac{k d v_x (v + v_B + v_y) \phi_o^2}{(v_o^2 + v_x^2 \phi_o^2)}\Big) \Big\}$$

which gives the cross spectrum and, when d is set to zero, it gives the Doppler spectrum. The exponential factor in the first row gives the reduced magnitude of the cross spectrum compared with the Doppler spectrum. That factor equals unity when $d = 0$ for the Doppler spectrum. The next two terms give the advancing and receding Bragg lines. The first exponential in each of those terms gives the line shape and the second exponential gives the phase factor for the cross spectrum. That phase factor does not exist in the Doppler spectrum, for which we take $d = 0$.

By taking the Fourier transform of (4), we obtain the autocorrelation and cross-correlation,

$$C(t) \sim 2\pi v_o \phi_o \; exp\Big(-\frac{(k d v_o \phi_o)^2}{2(v_o^2 + v_x^2 \phi_o^2)}\Big)$$

$$\Big\{ s_+ exp\big(ik(-v_B + v_y)t\big) \; + s_- exp\big(ik(+v_B + v_y)t\big) \Big\} \tag{5}$$

$$exp\left(-\frac{k^2}{2}(v_o^2 + v_x^2 \phi_o^2) \left(t + \frac{d v_x \phi_o^2}{v_o^2 + v_x^2 \phi_o^2} \right)^2 \right)$$

where t is the lag time and the autocorrelation is obtained by setting $d = 0$.

The radial velocity v_y is derived from the Doppler shift of the Bragg lines in the Doppler spectrum, which is obtained for either receiver by setting $d = 0$ in (4). The average position and shape of the Bragg lines are described by the second exponential function in (4). It shows that the Bragg lines are broadened by random surface current velocity variations v_o within the scattering patch and by the transverse current velocity v_x due to finite antenna beamwidth ϕ_o. That broadening can reduce the accuracy of the radial velocity estimate by increasing the error in locating the peaks of the Doppler-shifted Bragg lines. The radial velocity enters the autocorrelation through the phase.

The transverse velocity v_x can be derived from either the cross spectrum (4) or the cross-correlation (5). First, we show the standard method using the latter. Then, we demonstrate how the transverse velocity is derived from the cross spectrum.

The conventional formula for the transverse velocity (May et al., 1989) is

$$v_x = \frac{-\,d\,\tau'}{\tau'^2 + \tau_x^2} \tag{6}$$

where τ' is the lag of the peak in the cross-correlation and τ_x is where the autocorrelation amplitude drops from a peak value at $t = 0$ to the level of the cross-correlation maximum amplitude. The distance d, rather than the separation $2d$ of the receiving antennas, appears here because of the geometric doubling for backscattering (2). If a "target" moves a distance x, then the backscattered field pattern will move a distance $2x$.

We can derive this formula (6) from (5), which shows that

$$\tau_x = \frac{d\,v_o\,\phi_o}{v_o^2 + v_x^2\,\phi_o^2} \tag{7}$$

and

$$\tau' = \frac{-\,d\,v_x\,\phi_o^2}{v_o^2 + v_x^2\,\phi_o^2}. \tag{8}$$

Keep in mind that (6) is applied in general, whereas the results (7) and (8) were derived for the simple model of uniform current with Gaussian random fluctuations. Does (6) apply for other more complicated current models that might exist in coastal regions? Probably not, as this analysis assumed uniform currents with no curvature.

Now consider the cross spectrum (4), which can be used to derive the following alternative formula:

$$v_x = \frac{k\,d\,v_1^2\,s_{cs}}{a_{cs} + s_{cs}^2\,v_1^2} \tag{9}$$

where s_{cs} is the slope of the phase of the cross spectrum as a function of Doppler velocity,

$$s_{cs} = \frac{k d v_x \phi_o^2}{v_1^2} \tag{10}$$

where

$$v_1^2 = v_o^2 + v_x^2\,\phi_o^2 \tag{11}$$

is computed from the width of the Bragg line, which is the same for both the Doppler spectrum and the cross-correlation, and where

$$a_{cs} = \frac{(k\ d\ v_o\ \phi_o)^2}{v_1^2} \tag{12}$$

is computed from the ratio of the amplitude of the cross spectrum to that of the Doppler spectrum. Keep in mind that these results were derived for a uniform flow with Gaussian random variations. They would not be expected to apply in general for more complicated circulation patterns (Røyrvik, 1983). In the case of complicated flows, the SA method may not even give the mean current. Furthermore, if the current is rotating everywhere about the radar with no radial velocity component anywhere in the antenna beam, then no flow is detectable.

3. MEASUREMENTS

On 16 November 1988, radar measurements were made from 0530 to 1445 UTC. Time series with 512 points spaced 0.5 s apart (just over 4 min) were taken simultaneously on two receiving antennas every 15 min at six ranges along the antenna boresights starting with 1.5 km from the radar and separated by 0.9 km intervals. Radar hardware and computer software limitations prevented antenna beam steering and restricted the number of ranges and the lengths of the time series. In the next experiment, beam steering, more ranges, and longer time series will be implemented.

All of the data presented in this paper were averaged over 2 hours (eight samples) in order to reduce the variance in the cross-correlation and cross spectrum. Two-hour time averages are undesirable when the currents are changing rapidly, which they sometimes appeared to do in the Santa Barbara Channel during our observations. Without this averaging, the variation in the computed transverse current components was so large that we observed numerical instabilities in the method. The next experiment will allow more frequent sampling so that shorter time averages can be used.

Figure 2 shows a typical Doppler spectrum, autocorrelation, and cross-correlation taken during a time when the radar apparently made good measurements for both the radial and transverse current components. The Doppler spectrum contains two strong, broad lines that are shifted slightly to the left of the upper tick marks indicating the locations of advancing and receding Bragg lines in the absence of currents. This shift indicates the presence of a small current component away from the radar. Meanwhile, the cross-correlation (bottom of Fig. 2) shows a positive time lag, which indicates a transverse current component going from right to left across the antenna boresight. The high frequency structure on both the cross-correlation and autocorrelation are produced by the mixing of signals from the advancing and receding Bragg lines (5). That structure

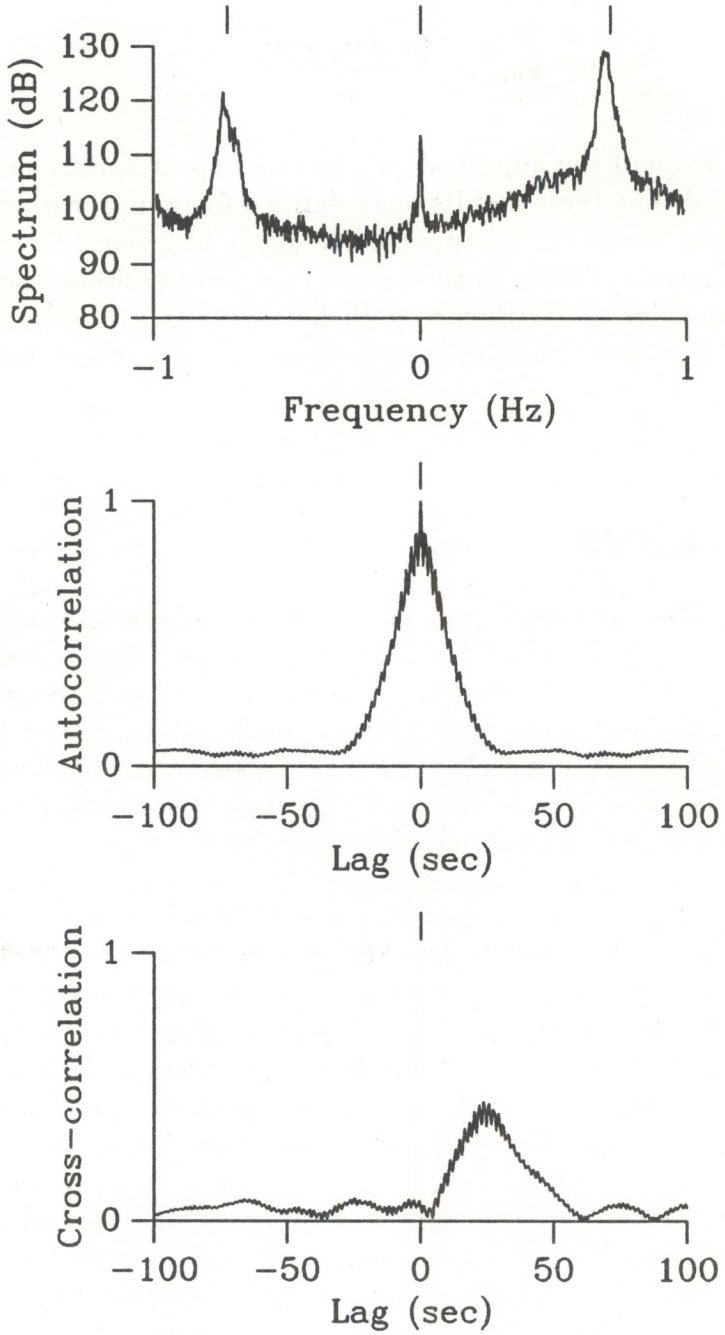

Fig. 2. The Doppler spectrum, autocorrelation, and cross-correlation for the first range gate (1.45 km), averaged from 0630 to 0830 on 16 November 1988. In each case, the average consisted of eight samples spaced 15 min apart. Each sample was derived from a time series of 512 points at intervals of 0.5 s. This is an example of measurements that produced a reliable transverse velocity component.

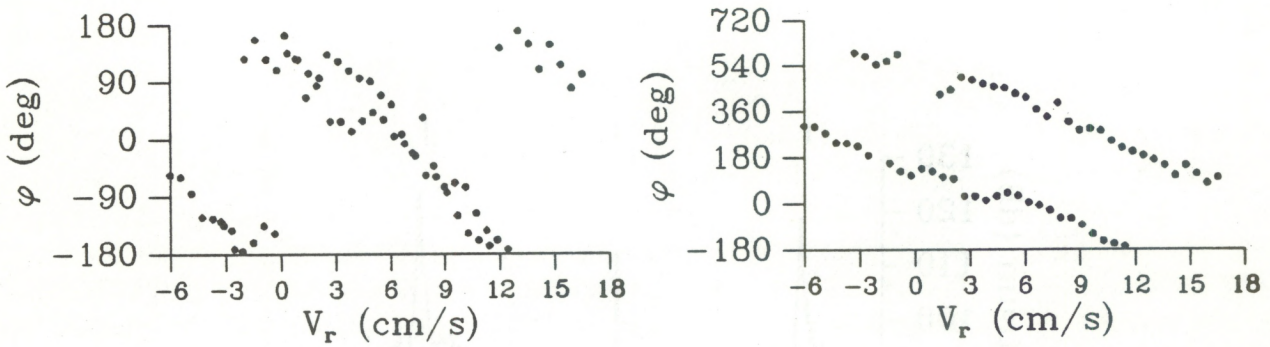

Fig. 3. The phase of the advancing and receding Bragg lines in the cross spectrum corresponding to data in Fig. 2. The left figure shows that phase before de-aliasing and editing. The right figure shows that phase afterwards.

has a smaller amplitude when the energy in one line is much greater than that in the other. The amplitude of that structure is greatest when the energy in both Bragg lines is the same.

The phase of the cross spectrum corresponding to the data in Fig. 2 is shown in Fig. 3. We see the expected linear relationship between the phase and the Doppler shift across the Bragg lines (4). Note that the phase in the upper frame appears to be aliased. Therefore, we had to de-alias it before computing the phase slope (10). Furthermore, we had to remove some bad points (using an editing technique developed by Wuertz and Weber, 1989) that were apparently caused by phase noise. Although that noise is not too large in this case, it was sometimes so large that the phase slope calculation was unstable.

Figure 4 shows an example when the SA method did not work as well as the previous example. Note that the high frequency structure on the autocorrelation and cross-correlation is larger than in Fig. 2. The Doppler spectra in both figures tell why. The receding and advancing Bragg lines have nearly the same energy in this case (Fig. 4), whereas the advancing line is much stronger in the earlier case (Fig. 2). Here the cross-correlation has no perceptible maximum, destabilizing the computation of the transverse velocity using the standard method (6). From the narrowness of the Bragg lines in the Doppler spectrum, we might guess that the transverse current component is weak. The widths of the Bragg lines put an upper limit on the transverse velocity component (May et al., 1988). Looking at the phase of the cross spectrum (Fig. 5), it is difficult to see clearly a straight line, which would make the computation of the transverse component using the phase slope method (9) difficult. We expect a nearly horizontal line in small currents. When this happens phase noise can present a real problem with this method. Averaging is intended to suppress the phase noise. Note also that there are fewer points in the phase plot with narrow Bragg lines (Fig. 5) than in the plot with broad Bragg lines (Fig. 3). That also affects the reliability of the small current measurements.

The radial component of surface current velocity in the first example (Figs. 2 and 3) is 0.6 cm s^{-1}. The transverse component is –21.3, –16.5, and –17.9 cm s^{-1} as computed

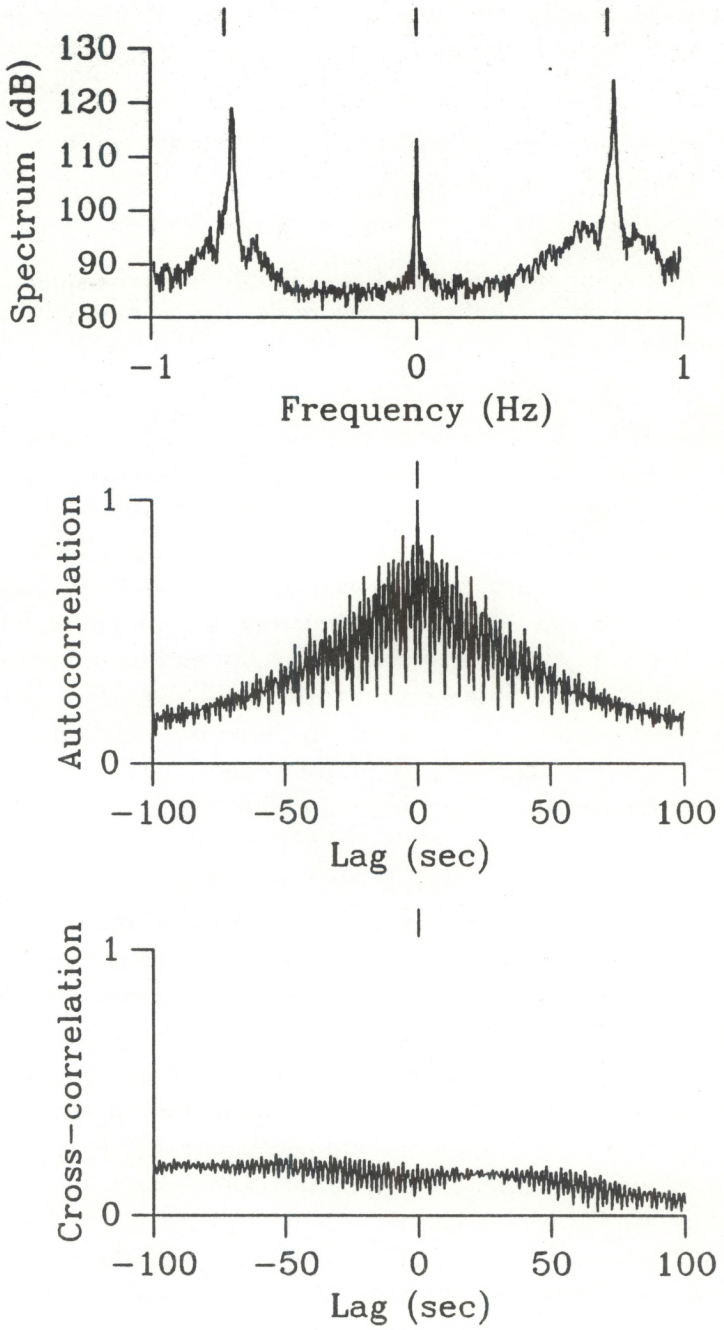

Fig. 4. The Doppler spectrum, autocorrelation, and cross-correlation for the fifth range gate (5.05 km), averaged from 1300 to 1500 on 16 November, 1988. In each case, the average consisted of eight samples spaced 15 min apart. Each sample was derived from a time series of 512 points at intervals of 0.5 s. This is an example of measurements that produced an unreliable transverse velocity component.

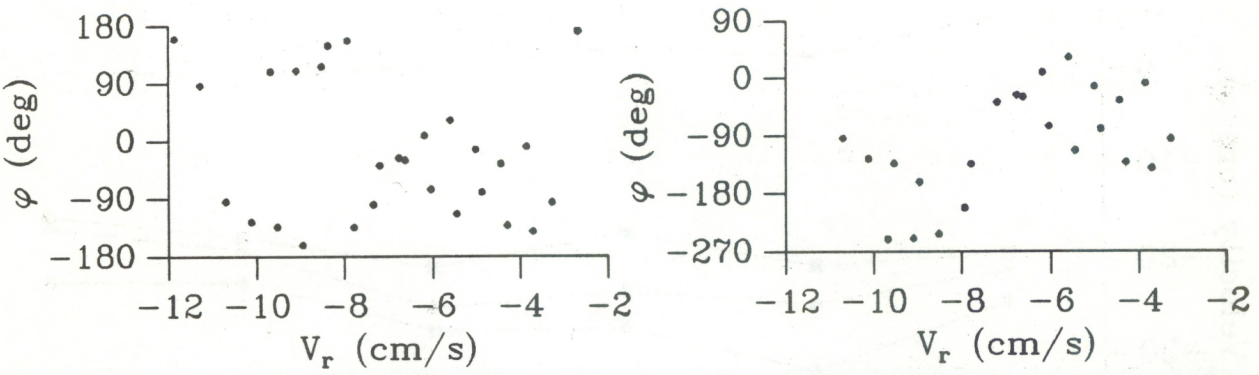

Fig. 5. The phase of the advancing and receding Bragg lines in the cross-spectrum corresponding to data in Fig. 4. The left figure shows that phase before de-aliasing and editing. The right figure shows that phase afterwards.

by three different methods: (*i*) the simplified standard formula (6) assuming $\tau_x = 0$ (this corresponds to the "apparent velocity" which is recognized to give an over-estimate), (*ii*) the standard formula using the width of the autocorrelation to compute τ_x, and (*iii*) the phase formula with the cross spectrum (9), respectively. The average of the three is –18.6 cm s^{-1} with a standard deviation of 2.0 cm s^{-1}.

The radial component in the second example (Figs. 4 and 5) is –6.8 cm s^{-1}. The transverse component is 6.7, 2.7, and 14.4 cm s^{-1} as computed by the three different methods. The average of the three is 7.9 cm s^{-1} with a standard deviation of 4.9 cm s^{-1}. This case demonstrates the instability of the SA technique when a distinguishable peak in the cross-correlation cannot be found and the phase of the cross spectrum is noisy. Judging from the narrowness of the Bragg lines, we believe that this is a case of such small transverse velocity that the backscattered pattern decorrelates by the time it translates from one receiving antenna to the next. There were other cases with even larger variances in the three measurements. Perhaps the receiving antennas could be spaced more closely together in weak currents. We expect all three methods to produce the same transverse velocity under ideal conditions when the velocity is uniform across the antenna beam and when there is no noise. Therefore, when the three methods produce significantly different results we suspect that actual conditions deviate from this ideal and the SA computation is unreliable. We anticipate making further improvements in stabilizing this computation. In contrast, the radial velocity measurement using the Doppler spectrum is very stable because that involves the computation of a simple shift in the positions of the Bragg lines.

Fig. 6 illustrates the measurement of the transverse current component as a function of range at a time when the three different methods showed consistency. Two methods used the standard formula with the cross-correlation (6). But the simplified standard method giving the apparent velocity did not use the width of the autocorrelation (7), by assuming $\tau_x = 0$. When those two methods agree, the results from the SA technique are generally accepted, although it is well known that the apparent velocity is an over estimate. The third method used the phase formula with the cross spectrum (9). It gave measurements in between the other two. Finally, Fig. 7 shows the measurements as a function of time

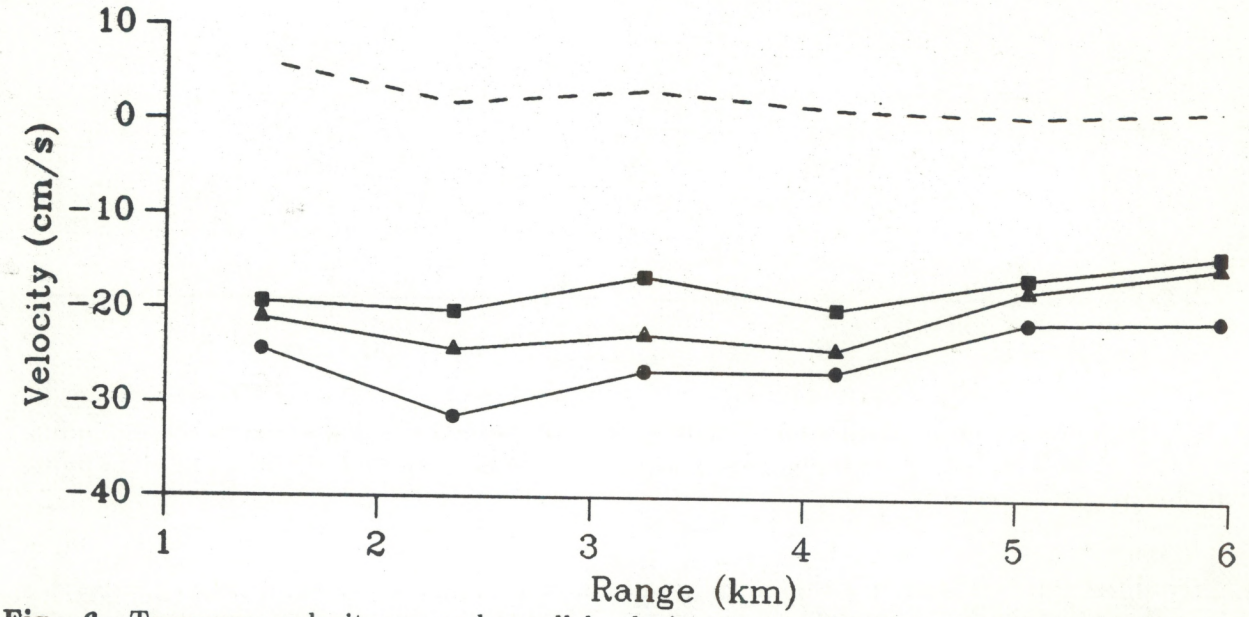

Fig. 6. Transverse velocity v_x and parallel velocity v_y as a function of range, averaged from 0630 to 0830 on 16 November 1988. The dashed line gives v_y, while the other three lines give v_x derived with different methods. The line with circular symbols was derived using the simplified standard method, i.e., (6) with $\tau_x = 0$. The line with square symbols was derived with the standard method (6). The line with triangular symbols was derived using the cross-correlation phase (9).

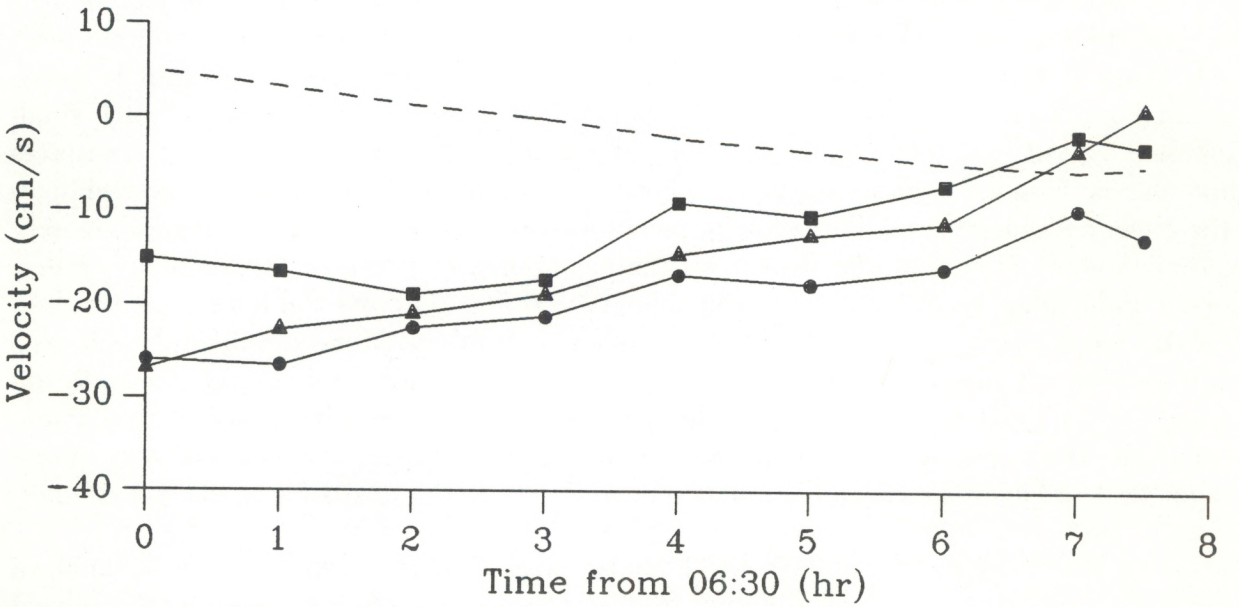

Fig. 7. Transverse velocity v_x and parallel velocity v_y as a function of time from 0630 to 1400 on 16 November 1988 at a range of 3.3 km. The dashed line gives v_y, while the other three lines give v_x derived with different methods. The line with circular symbols was derived using the simplified standard method, i.e., (6) with $\tau_x = 0$. The line with square symbols was derived with the standard method (6). The line with triangular symbols was derived using the cross-correlation phase (9).

at one range. All three methods showed consistency as a function of both range and time. However, their differences are a sizeable fraction of the estimated transverse velocity component. Some of the SA methods employed here may contain biases that are not important for the high winds observed in the atmosphere but which are noticeable for the smaller currents observed in the ocean.

4. CONCLUSIONS

This experiment accomplished one of its modest goals: to demonstrate the SA method of measuring transverse currents on the surface of the ocean. But it also raises some questions about the applicability of the method in weak currents. The SA method has been applied for years in the measurement of winds in the atmosphere, where the winds are typically much stronger than ocean currents. Is there a lower velocity limit below which this method is impractical? That is one of the important questions we hope to answer in the next experiment and with further theoretical analysis.

Another potential problem is related to antenna beamwidth. With the Doppler method, narrower beams give better spatial resolution and better velocity resolution at the same time, whereas, the SA method relies upon the finite beamwidth of the antennas in order to sense the transverse current component. Broadening the antenna beam can help in the measurement of that component, but at the expense of spatial resolution. And when the circulation pattern in coastal waters is complicated, the velocity is no longer uniform across the antenna beam, violating a fundamental assumption of the technique.

In spite of these problems, we feel that the method is worth pursuing because of the potential benefits of single station operation. Those benefits are gained at the expense of more complicated analysis and greater sensitivity to noise. Therefore, our next experiment will be designed to better evaluate the accuracy and the limitations of the single station Doppler / Spaced Antenna radar.

APPENDIX

The received RF signal scattered from the ocean surface can be viewed as a superposition of plane waves as follows.

$$E(\boldsymbol{r},t) = \int d^2k_s \; d\omega_s \; E(\boldsymbol{k}_s,\omega_s) \; exp \; i(\boldsymbol{k}_s \cdot \boldsymbol{r}_s - \omega_s t) \qquad \text{(A-1)}$$

where t is the time of reception by an antenna located at position $\boldsymbol{r}$ relative to the transmitter antenna. This integral includes all scattered RF waves coming from different directions within the radar antenna beam.

It is assumed that the scatter is caused by ocean surface waves, where the wavevector of each scattered wave is

$$\boldsymbol{k}_s = \boldsymbol{k}_i + \boldsymbol{k} \tag{A-2}$$

where $\boldsymbol{k}_i$ is the wavevector of the transmitted RF wave incident upon the ocean and where $\boldsymbol{k}$ is the wavevector of the ocean surface wave doing the scattering. All of these wavevectors are taken to be positive when pointing away from the radar.

The ocean wavevector $\boldsymbol{k}$ determines the scattering geometry. For near backscattering,

$$\boldsymbol{k}_s \simeq -\boldsymbol{k}_i \simeq \boldsymbol{k}/2 \; . \tag{A-3}$$

Thus, backscatter is produced by ocean waves (Bragg waves) with wavelengths equal to half the RF wavelength and propagating radially either towards or away from the radar. As a result, a different ocean wave is involved in the backscattering at different azimuth angles within the antenna beam.

The wave frequency of each scattered component is

$$\omega_s = \omega_i + \omega_d \tag{A-4}$$

where ω_i is the wave frequency of the transmitted RF wave incident upon the ocean and where ω_d is the frequency Doppler shift, which equals the frequency for the ocean surface wave doing the scattering,

$$\omega_d = \pm\omega_B + \boldsymbol{k} \cdot \boldsymbol{v} \tag{A-5}$$

where ω_B is the Bragg frequency $\sqrt{gk}$, with the plus sign for waves propagating towards the radar and the minus sign for waves propagating away from the radar. Thus, in general, the backscatter Doppler spectrum contains two dominant lines called the receding and advancing Bragg lines corresponding to ocean waves propagating away from and toward the radar. The Doppler shifts of those lines are due to the phase velocities of these Bragg waves plus the velocity of any surface current. The ocean surface current $\boldsymbol{v}$ is positive going away from the radar. Therefore, since $\boldsymbol{k}$ (A–3) is negative toward the radar, currents toward the radar will cause additional positive Doppler shifts.

The position of each RF receiver relative to the transmitter antenna is denoted by

$$\boldsymbol{r} = \boldsymbol{r}_i + \boldsymbol{r}_s \tag{A-6}$$

where $\boldsymbol{r}_i$ is the location of the scattering ocean wave relative to the transmitter and where $\boldsymbol{r}_s$ is the location of the receiver relative to the scattering ocean wave. Now, the transmitter and receiver antennas are closely spaced together compared with the distance to the

scattering target and, as a result, the received radar signal can be attributed entirely to near backscattering. Then, $\boldsymbol{r}_s \simeq -\boldsymbol{r}_i$ and both are much larger in magnitude than $\boldsymbol{r}$.

Therefore, the backscattered RF received signal (A–1) can be represented by

$$E(\boldsymbol{r},t) \sim exp\, i(\boldsymbol{k}_i \cdot \boldsymbol{r}_i - \omega_i t) \int dv_r \Big(E_+(\boldsymbol{k},v_r)\, exp(-i\omega_B t) + E_-(\boldsymbol{k},v_r)\, exp(+i\omega_B t) \Big) exp\big(i\boldsymbol{k} \cdot (\boldsymbol{r}/2 - \boldsymbol{v}t)\big) \tag{A–7}$$

where v_r is the radial component of surface current velocity defined by $kv_r = -\boldsymbol{k} \cdot \boldsymbol{v}$ and where $E_\pm$ gives the strengths of the received signals in the advancing/receding Bragg lines, which are proportional to the waveheights of the advancing/receding ocean surface waves causing the backscattering. They are also proportional to the directional antenna gain.

This integral (A–7) is over the radial component of current velocity, which replaces the scattered frequency (A–4). This current can vary as a function of position inside the radar scattering patch, so that the integral is actually over the area of that patch. Furthermore, the exponential factor in front of the integral will be ignored since it is not important for this analysis and is removed through RF signal processing, e.g., the transmitted frequency ω_i is removed from the received signal through mixing with the local oscillator.

A spectral analysis of the received signal (A–7) gives the radar Doppler spectrum,

$$S(\boldsymbol{r},\omega) = E(\boldsymbol{r},\omega)E^*(\boldsymbol{r},\omega) \sim \int dv_r\; S_\pm(\boldsymbol{k},v_r)\; \delta(\omega - \omega_d) \tag{A–8}$$

in which $S_\pm(\boldsymbol{k},v_r) = E_\pm(\boldsymbol{k},v_r)E^*_\pm(\boldsymbol{k},v_r)$ is the ocean wave spectrum and where the asterisk indicates the complex conjugate. Take special note of the fact that this spectrum is the same for both receiver antennas. The only difference in their received signals enters through the phase (A–7) because of the difference in their locations $\boldsymbol{r}$. That phase information is lost in the power spectrum of both receivers.

The Doppler spectrum and the ocean wave spectrum in (A–8) are sometimes defined using an ensemble average over randomly varying components. However, the integral relation (A–8) follows directly from (A–7) without any statistical averaging. This is because the time series (A–7) contains a superposition of sinusoids caused by backscattering from ocean waves. And, sinusoidal time series lead to delta functions in the Doppler spectrum (A–8).

We obtain the autocorrelation by taking the inverse Fourier transform of the Doppler

spectrum (A–8). That is,

$$
\begin{aligned}
C(\boldsymbol{r},t) &= \int_{-\infty}^{+\infty} d\tau\ E(\boldsymbol{r},t+\tau)E^{*}(\boldsymbol{r},\tau) \\
&= 2\pi \int_{-\infty}^{+\infty} d\omega\ S(\boldsymbol{r},\omega)\ exp(-i\omega t) \\
&\sim \int dv_r \Big(S_{+}(\boldsymbol{k},v_r)\ exp\big(-i\omega_B t\big) \\
&\quad + S_{-}(\boldsymbol{k},v_r)\ exp\big(+i\omega_B t\big)\Big) exp - i\boldsymbol{k}\cdot\boldsymbol{v}t
\end{aligned}
\tag{A–9}
$$

which shows that the antenna position-dependent phase term in (A–7) is also lost in the autocorrelation. The autocorrelation and the Doppler spectrum provide complementary pictures. One may be preferred over the other for particular applications, but they both contain the same information, just in different forms. The spectrum (A–8) is useful in separating signals when their Doppler-shifted frequencies are recognizably different. Those same signals are not separated in the autocorrelation.

The cross spectrum is formed by taking the product of the amplitude spectra for the two receivers. That is,

$$
\begin{aligned}
S(\boldsymbol{r}_{12},\omega) &= E(\boldsymbol{r}_1,\omega)E^{*}(\boldsymbol{r}_2,\omega) \\
&\sim \int dv_r\ S_{\pm}(\boldsymbol{k},v_r)\ \delta(\omega-\omega_d) exp\ i\boldsymbol{k}\cdot\boldsymbol{r}_{12}/2
\end{aligned}
\tag{A–10}
$$

which is identical to the power spectrum (A–8) except for the phase containing the separation of the two receiver antennas, $\boldsymbol{r}_{12} = \boldsymbol{r}_1 - \boldsymbol{r}_2$, where the subscripts 1 and 2 denote the two receiver antennas. This phase is larger for larger separations between the receiving antennas and it is a function of the directions for the backscattering ocean waves. This phase factor is at the heart of the spaced-antenna method.

We obtain the cross-correlation by taking the inverse Fourier transform of the cross

spectrum (A–10). That is,

$$
\begin{aligned}
C(\boldsymbol{r}_{12},t) &= \int_{-\infty}^{+\infty} d\tau\ E(\boldsymbol{r}_1,t+\tau)E^*(\boldsymbol{r}_2,\tau) \\
&= 2\pi \int_{-\infty}^{+\infty} d\omega\ S(\boldsymbol{r}_{12},\omega)\ exp(-i\omega t) \\
&\sim \int dv_r \left(S_+(\boldsymbol{k},v_r)\ exp\big(-i\omega_B t\big)\right. \\
&\left. + S_-(\boldsymbol{k},v_r)\ exp\big(+i\omega_B t\big)\right) exp\ i\boldsymbol{k}\cdot(\boldsymbol{r}_{12}/2-\boldsymbol{v}t)
\end{aligned}
\tag{A–11}
$$

which is identical to the autocorrelation (A–9) except for the phase factor containing the separation of the receiver antennas and the ocean wavevector. As with the Doppler spectrum and the autocorrelation, the cross spectrum and the cross-correlation provide complementary pictures.

REFERENCES

Barrick, D.E., M.W. Evans, and B.L. Weber, 1977: Ocean Surface Currents Mapped by Radar, *Science, 198*, 138-144.

Briggs, B.H., 1980: Radar Observations of Atmospheric Winds and Turbulence: a Comparison of Techniques, *J. Atmos. Terres. Phys., 42*, 823-833.

Briggs, B.H., 1984: The Analysis of Spaced Sensor Records by Correlation Techniques, Handbook for MAP, vol. 13, Ground-Based Techniques, Ed. R.A. Vincent, November, 166-186.

Frisch, A.S., and B.L. Weber, 1982: Applications of Dual-Doppler HF Radar Measurements of Ocean Surface Currents, *Remote Sensing of Environment, 12*, 273-282.

Frisch, A.S., and B.L. Weber, 1980: A New Technique for Measuring Tidal Currents by Using a Two-Site HF Doppler Radar System, *J. Geophys. Res., 85*, 485-493.

Hocking, W.K., P.T. May, and J. Röttger, 1989: Interpretation, Reliability and Accuracies of Parameters Deduced by the Spaced Antenna Method in Middle Atmosphere Applications, *Pure Appl. Geophys., 130*, 571-604.

Larsen, M.F., and J. Röttger, 1989: The Spaced Antenna Technique for Radar Wind Profiling, *J. Atmos. Ocean. Technol., 6*, 920-938.

May, P.T., 1988: Statistical Errors in the Determination of Wind Velocities by the Spaced Antenna Technique, *J. Atmos. Terres. Phys., 50*, 21-32.

May, P.T., 1989: Single Station Ocean Current Vector Measurement: Application of the Spaced Antenna (SA) Technique, *Geophys. Res. Letters, 16*, 999-1002.

May, P.T., 1990: Spaced Antenna vs. Doppler Radars: A Comparison of Techniques Revisited, (submitted to *Radio Science*).

May, P.T., S. Kato, S. Fukao, T. Tsuda, and T. Sato, 1988: Estimation of the Wind Component Normal to a Radar Beam, *J. Geomag. Geoelectr., 40*, 1047-1052.

Røyrvik, O., 1983: Spaced Antenna Drift at Jicamarca, Mesospheric Measurements, *Radio Science, 18*, 461-476.

Strauch, R.G., B.L. Weber, A.S. Frisch, C.G. Little, D.A. Merritt, K.P. Moran, and D.C. Welsh, 1987: The Precision and Relative Accuracy of Profiler Wind Measurements, *J. Atmos. Ocean. Technol., 4*, 563-571.

Vincent, R.A., P.T. May, W.K. Hocking, W.G. Elford, B.H. Candy, and B.H. Briggs, 1987: First Results with the Adelaide VHF Radar: Spaced Antenna Studies of Tropospheric Winds, *J. Atmos. Terres. Phys., 49*, 353-366.

Weber, B.L., and D.B. Wuertz, 1990: Comparison of Rawinsonde and Wind Profiler Radar Measurements, *J. Atmos. Ocean. Technol., 7*, 157-174.

Wuertz, D.B., B.L. Weber, R.G. Strauch, A.S. Frisch, C.G. Little, D.A. Merritt, K.P. Moran, and D.C. Welsh, 1988: Effects of Precipitation on UHF Wind Profiler Measurements, *J. Atmos. Ocean. Technol., 5*, 450-465.

Wuertz, D.B., and B.L. Weber, 1989: Editing Wind Profiler Measurements, NOAA Tech. Rep. ERL 438-WPL 62, NOAA Environmental Research Laboratories, Boulder, CO, 78 pp.

☆U.S. GOVERNMENT PRINTING OFFICE: 1991 - 573-002/21029